Ion storage in the rf octupole trap

J. Walz,* I. Siemers, M. Schubert, W. Neuhauser, and R. Blatt
Institut für Laser-Physik, Universität Hamburg, Jungiusstraße 9, 20355 Hamburg, Germany

E. Teloy
Fakultät für Physik, Universität Freiburg, Hermann-Herder-Straße 3, 79104 Freiburg, Germany
(Received 23 November 1993)

Confinement of ion clouds in an rf octupole ion trap is investigated with particular emphasis on the trapping stability, which is position dependent. Excitation spectra of trapped clouds of Ba^+ ions are observed, and the kinetic energy of ion clouds is derived. The spatial extension of ion clouds is measured, providing the basis for an experimental study of the trapping stability. For ion clouds in an rf octupole trap the mean kinetic energy is smaller and the spatial extension is larger than in comparable Paul traps.

PACS number(s): 32.80.Pj, 52.20.Dq

I. INTRODUCTION

Confinement of ions both in Paul and Penning traps has proved to be a most valuable tool for precision spectroscopy, time and frequency standards [1,2], and for experiments in quantum optics [3–5]. Unique features of ion traps, including long interaction times, absence of perturbations by collisions with confining walls and the possibility to localize particles to spatial extensions smaller than an optical wavelength, led to striking demonstrations in high resolution laser spectroscopy [6]. For ultimate accuracy and resolution, laser cooling of ions is needed [7]. With ion clouds this is successfully accomplished only in Penning traps, but the use of Penning traps is very often restricted due to the required high magnetic field, especially for heavy ions. In Paul traps, Coulomb interaction of trapped particles couples energy from the trapping rf field to the motion of particles. This rf heating [8] counteracts laser cooling of ion clouds in Paul traps [9].

For many spectroscopic applications it would be desirable to employ rf traps and load them with as many particles as possible with an energy as low as can be achieved. It has been suggested to use higher-order rf traps for storing higher particle numbers than possible in a Paul trap [10]. A higher-order rf trap has the additional advantage that the driven motion of trapped particles (micromotion) for most of the trap's volume is smaller than for Paul traps of comparable size. Hence it is expected that rf heating plays a lesser role, allowing for lower energies of trapped ion clouds. Since the trapping rf field of a higher-order trap is nonlinear, the trapping stability will be qualitatively different from the motion of particles in a Paul trap, governed by linear equations of motion. In this paper we present investigations on the trapping stability, space charge effects, and on the dynamics of ion clouds in a rf octupole trap. A brief account of work concerning the stability of a nonlinear parametric oscillator has been published elsewhere [11].

Multipole rf potentials have been used in ion sources and beam-guiding devices for measurements of total cross sections of ion-molecule reactions first by Teloy and Gerlich [12] and later by others [13–15]. Single-particle equations of motion in linear rf multipole fields have been studied to some extent [16], and detailed investigations of the transmission properties of linear rf octupole beam guides have been performed [15]. To our knowledge spectroscopic features and the dynamics of ion clouds in octupole traps have not been investigated so far.

This paper is organized as follows: in Sec. II the electrode structure and the electric potential of the rf octupole trap are given. The equations of motion are numerically integrated in Sec. III for an investigation of the trapping stability which is treated further with analytical arguments in Sec. IV. In Sec. V the space charge distribution of an ion cloud in the anharmonic pseudopotential is calculated. The experimental setup is described in Sec. VI and in Sec. VII the line shapes of excitation spectra are discussed. Measurements of the mean kinetic energy and the stored particle number as a function of the trapping parameters are presented in Sec. VIII. The observed spatial distribution of an ion cloud is shown in Sec. IX and, finally, the position dependence of the trapping stability is discussed in Sec. X.

II. THE RF OCTUPOLE TRAP

The electrode structure of the rf octupole trap is designed to generate the three-dimensional octupole potential (in spherical coordinates)

$$\Phi(r,\vartheta,\varphi) = A\, r^4\, P_4(\cos\vartheta). \tag{1}$$

Here, r, ϑ, and P_4 denote the elongation from the trap center, the polar angle and the fourth Legendre polynomial, respectively.

*Present address: Max Planck Institut für Quantenoptik, Hans-Kopfermann-Straße 1, 85748 Garching, Germany.

Figure 1 shows the realized trap configuration consisting of two endcaps and three ring electrodes (i.e., two intermediate rings and a central ring), where the rf potential $V_{RF} = V_0 \cos \Omega t$ is applied between adjacent electrodes.

In order to determine the constant factor A in Eq. (1) consider: (i) z_0 denoting half the inner distance between the endcaps, (ii) r_{in} denoting the closest distance of the intermediate ring electrodes to the trap's center at the polar angle $\vartheta = \arccos(\sqrt{3/7})$, and (iii) ρ_0 denoting half the inner diameter of the central ring. Voltages applied to the octupole trap can be written in a general way as $V_1 = \Phi(\text{endcap}) - \Phi(\text{intermediate ring})$ and $V_2 = \Phi(\text{endcap}) - \Phi(\text{central ring})$. Taking the difference $V_1 - V_2$ and evaluating the potential [Eq. (1)], the factor A follows as

$$A = \frac{V_1 - V_2}{s^4}, \tag{2}$$

where s denotes a characteristic trap dimension, given by

$$s^4 = \frac{3}{8}\rho_0^4 + \frac{3}{7}r_{in}^4. \tag{3}$$

For given trap dimensions ρ_0, r_{in}, and z_0 the voltages V_1 and V_2 cannot be chosen arbitrarily to generate an octupole potential. Taking the sum $V_1 + V_2$ and inserting Eqs. (2) and (3) gives

$$z_0^4 - \frac{3V_1}{8(V_1 - V_2)}\rho_0^4 - \frac{3V_2}{7(V_1 - V_2)}r_{in}^4 = 0. \tag{4}$$

If no voltage is applied between the endcaps and the (central) ring electrode, i.e., $V_2 = 0$, the ratio ρ_0/z_0 follows from Eq. (4),

$$\frac{\rho_0}{z_0} = (8/3)^{1/4} \approx 1.28. \tag{5}$$

A convenient choice of the ratio r_{in}/z_0 follows from the condition $\Phi(\text{endcap}) = -\Phi(\text{intermediate ring})$ which is arbitrary in the sense that only potential differences have physical reality, and is given by

$$\frac{r_{in}}{z_0} = (7/3)^{1/4} \approx 1.24. \tag{6}$$

This corresponds to the choice $\rho_0/z_0 = \sqrt{2}$ for the electrodes of a quadrupole trap, there resulting from the condition $\Phi(\text{endcap}) = -\Phi(\text{ring})$ [17]. For $V_2 = 0$, and for a choice according to Eqs. (4), (5), and (6) the rf octupole potential is eventually given in cylindrical coordinates by

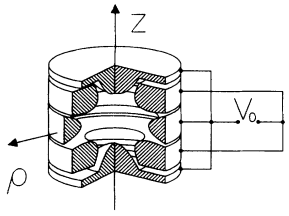

FIG. 1. Electrode structure of the rf octupole trap.

$$\Phi(\rho, \varphi, z) = \frac{V_0 \cos(\Omega t)}{2z_0^4}\left(\frac{3}{8}\rho^4 - 3\rho^2 z^2 + z^4\right). \tag{7}$$

Note that only ac potentials are considered throughout this paper. Added dc potentials merely complicate the treatment, and in the experiment they proved to deteriorate the trap stability.

III. NUMERICAL INTEGRATION OF THE EQUATIONS OF MOTION

The equations of motion for a single particle of mass m and charge q in the three-dimensional rf octupole are given by

$$\frac{d^2}{d\nu^2}\frac{\rho}{s} = 2q_4 \cos(2\nu)\frac{3}{\sqrt{2}}\frac{\rho}{s}\left(\frac{\rho^2}{2s^2} - 2\frac{z^2}{s^2}\right) + \frac{4M_z^2}{m^2\Omega^2\rho^3 s}, \tag{8a}$$

$$\frac{d^2}{d\nu^2}\frac{z}{s} = 2q_4 \cos(2\nu)\sqrt{2}\frac{z}{s}\left(3\frac{\rho^2}{z^2} - 2\frac{z^2}{s^2}\right), \tag{8b}$$

where time t is scaled to the trap's driving frequency by $\nu = t\Omega/2$. The rf voltage is scaled according to

$$q_4 = 2\sqrt{2}\frac{qV_0}{m\Omega^2 s^2}. \tag{9}$$

M_z denotes the angular momentum of the particle with respect to the z axis,

$$M_z = m\rho^2\dot{\varphi}. \tag{10}$$

The equations of motion (8) take the form of two nonlinear, coupled, and explicitly time-dependent differential equations. Hence it is not possible in a straightforward way to give a general theory of motional stability and one has to rely either on numerical integration of the equations of motion or approximate analytical arguments.

Figure 2 shows the radial projection of the motion of a single particle in the rf octupole trap, obtained by numerical integration of the equations of motion (8) for 70 periods of the driving frequency $\Omega/2\pi$. The initial conditions were $\rho/z = 0.1$, $z/s = 0.1$, $d\rho_s/dz = 0$, $dz/d\nu = 0$ at $\nu = 0$. The scaled rf voltage was set to $q_4 = 6.0$ and the angular momentum M_z was assumed to be zero. Near the center of the rf octupole trap the potential depends only weakly on the spatial extension, hence the ion motion is only weakly affected by the trapping field. In Fig. 2 this leads to extended straight sections of the ion motion around the center of the ion trap. For larger elongation the octupole potential gets steep and the ion experiences a strong ponderomotive restoring force which shows up in Fig. 2 as a micromotion near the maximum amplitude. The particular trajectory shown in Fig. 2 subsequently becomes unstable: after approximately 220 periods of the driving frequency Ω, the maximum velocity increases quickly and the ion eventually is lost by a collision with the trap electrodes.

It should be mentioned at this point that single ion

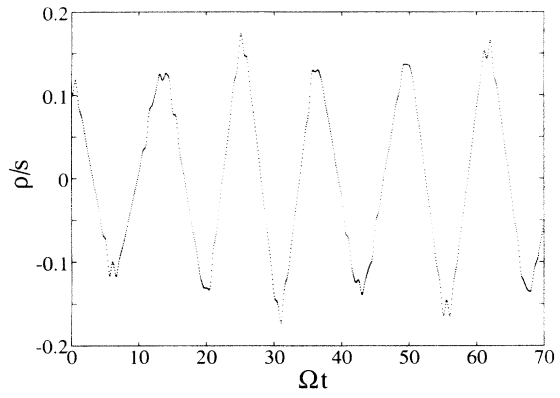

FIG. 2. Radial projection of the motion of a single particle in the rf octupole trap, obtained by numerical integration of the equations of motion for 70 periods of the rf driving frequency $\Omega/2\pi$. The initial conditions are $\rho/z = 0.1$, $z/s = 0.1$, $d\rho/dz = 0$, $dz/d\nu = 0$ at $\nu = 0$, the scaled rf voltage was set to $q_4 = 6.0$ and the angular momentum M_z was assumed to be zero.

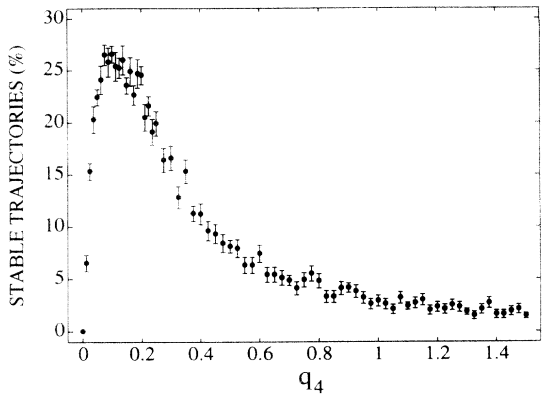

FIG. 3. Result of a Monte Carlo simulation of the trapping stability. The parameters were chosen according to experimental conditions and were set to $s = 17.6$ mm, $\Omega/2\pi = 400$ kHz, and the trapping volume is ellipsoidal with a radial diameter of $1.6s$ and an axial diameter of $2.26s$.

motion may exhibit chaotic dynamics in the rf octupole trap, but not in the Paul trap. (Motion of two and more ions in the Paul trap may be chaotic due to Coulomb interaction [9].) A detailed study of chaotic dynamics is beyond the scope of this paper and is not pursued here.

To study the trapping stability for ions in the rf octupole trap, as a first approach we used the following procedure: for a large number of single particle trajectories the initial position is chosen from a homogeneous distribution over the trap volume and initial velocities are randomly determined according to a Maxwell-Boltzmann distribution. The equations of motion are then integrated for a large (somehow arbitrary) number of periods of the trap frequency $\Omega/2\pi$ and the fraction of trajectories which do not leave the trapping volume is taken as a measure for the stability of ion confinement in the rf octupole trap. Figure 3 shows the result of such a Monte Carlo calculation for the stability of a single particle in the rf octupole trap. The parameters for these calculations were chosen as realized in the experimental setup (cf. Sec. VI below), and are given by $s = 17.6$ mm, $\Omega/2\pi = 400$ kHz. The trapping volume is ellipsoidal with radial diameter $1.6s$ and axial diameter $2.26s$. The mean temperature for the Maxwell-Boltzmann distribution was set to 700 K and the motion of the particle was followed during 500 periods of the rf trapping voltage. The stability of the rf octupole trap shows a maximum at values of the scaled trapping voltage of about $q_4 = 0.1$. For higher rf voltages the motion of the ions with large distances to the trap center becomes increasingly unstable. Energy from the driving field is coupled to the ion motion thus increasing the size of the ion orbit and eventually the ion is lost due to a collision with one of the electrodes. Hence the acceptance of the rf octupole trap decreases for high rf voltages. On the other hand, for very low rf voltages ions may get lost if the pondermotive force at the border of the trapping volume is too weak to reflect ions with thermal energy back towards the center of the trap. Hence, the acceptance of the rf octupole trap decreases for low rf voltages. The foregoing interpretation of the numerical results for the motional stability of ions in the rf octupole trap is upheld by analytical arguments in the following section.

IV. MOTIONAL STABILITY IN AN ANHARMONIC RF POTENTIAL

For comparison, we consider first the stability analysis for a Paul trap. The motion of charged particles in a Paul trap is described by linear, uncoupled, and explicitly time-dependent equations of motion (Mathieu equations). Using Floquet theory, the equations of motion can be solved analytically. The stability of a particle's motion depends only on the parameters a_z and q_z, which denote scaled dc and rf voltages, respectively. In the parameter plane (a_z, q_z) distinct regions allowing for stable motion exist. Stability for the motion in a Paul trap means that a trajectory with arbitrary initial conditions does not leave a limited spatial region. (For real Paul traps, initial conditions, of course, cannot be arbitrary, since particles may get lost by hitting the trap's electrodes.)

The motion of charged particles in a higher-order rf trap is described by nonlinear, coupled, and explicitly time-dependent equations of motion. The only conserved quantity is the angular momentum with respect to the axis of an electrode structure having rotational symmetry. Aside from singular periodic orbits, stability in the same sense as in the stability-analysis for a Paul trap does not exist. Instead, the time a particle is staying in the trap's volume and the changing of it's energy is considered, which is also more relevant for practical applications. It turns out that the stability of a particle's motion depends strongly on it's initial energy. In the following, we describe the procedure to estimate motional stability for higher-order rf traps, which has been successfully applied since the first experiments on this subject [12].

A dimensionless stability function [12], which is pro-

portional to the local quadrupole field strength, is defined according to

$$\eta(\vec{r}) = \left| \frac{2q}{m\Omega^2} \vec{\nabla} |\vec{E}(\vec{r})| \right|. \tag{11}$$

Note that a similar approach employing the concept of local quadrupole field strength has been pursued by Wineland for proposed linear multipole rf traps [10].

In the case of the electric field of the Paul trap

$$\vec{E}_{\text{Paul}}(r, \vartheta, \phi) = -\vec{\nabla} \frac{V_0}{r_0^2 + 2z_0^2} r^2 (1 - 3\cos^2 \vartheta) \tag{12}$$

the stability function $\eta(\vec{r})$ is given in spherical coordinates by

$$\eta_{\text{Paul}}(\vartheta) = \frac{4qV_0}{m\Omega^2(r_0^2 + 2z_0^2)} \left[\frac{1 + 15\cos^2 \vartheta}{1 + 3\cos^2 \vartheta} \right]^{1/2}. \tag{13}$$

Due to the linearity of the equations of motion the stability of a charged particle in the Paul trap does not depend on the distance at which the particle is from the trap's center. Correspondingly, η_{Paul} does not depend on r. The stability function η_{Paul} depends only on the polar angle ϑ, since the slope of the electric field in a Paul trap in axial direction is minus twice the slope in radial direction. In the radial and in the axial direction, η_{Paul} equals the Mathieu parameters q_r and q_z, respectively [18]. These parameters are determined by the ratio of the secular frequencies and the trapping frequency, i.e., $q_{r,z} = 2\sqrt{2}\, \omega_{r,z}/\Omega$.

As an alternative to the concept of a local quadrupole field strength, the stability function $\eta(\vec{r})$ can also be viewed as characterizing the validity of the adiabatic (pseudopotential) approximation [19,20], which has been discussed in [11,12]. Yet another aspect of the stability function $\eta(\vec{r})$ is obtained by evaluating the ratio of the modulus of the effective restoring force

$$\left| \vec{F}_{\text{pseudo}}(\vec{r}) \right| = \left| \vec{\nabla} \Psi(\vec{r}) \right| \tag{14}$$

due to the trap's pseudopotential,

$$\Psi(\vec{r}) = \frac{q}{4m\Omega^2} \left[\vec{E}(\vec{r}) \right]^2, \tag{15}$$

and the maximum force due to the trap's rf field,

$$\left| \vec{F}_{\text{rf,max}}(\vec{r}) \right| = q \left| \vec{E}(\vec{r}) \right|, \tag{16}$$

which yields

$$\frac{\left| \vec{F}_{\text{pseudo}}(\vec{r}) \right|}{\left| \vec{F}_{\text{rf,max}}(\vec{r}) \right|} = \frac{1}{4} \eta(\vec{r}). \tag{17}$$

Since the trap's pseudopotential is generated by the rf field, this ratio might be viewed as a force-conversion coefficient. As evidenced by Eq. (17), the stability function $\eta(\vec{r})$ is proportional to the force-conversion coefficient. This again relates to the validity of the adiabatic approximation, where the force-conversion coefficient should be small compared to unity.

Most important for practical trap design is that the stability parameter $\eta(\vec{r})$ determines the amount of energy coupled from the driving field to the ion motion. This can be obtained from numerical calculations of particle trajectories starting near the trap center in the following way: Taking the difference ΔH between the initial energy H and the energy after a reflection by the trap potential, the maximum energy gain $\max|\Delta H/H|$ can be determined. The logarithm of $\max|\Delta H/H|$ for any rf multipole trapping configuration exhibits a characteristic linear dependence on the inverse maximum value of the stability parameter [21]. This is shown in Fig. 4 for the rf octupole trap. For large $\eta_{\max}$, the maximum energy transfer increases and the trap stability decreases.

In the adiabatic approximation the trajectories of particles can reach at most the surface where the pseudopotential energy equals their initial energy. Hence the maximum of the stability function $\eta(\vec{r})$ in the case of rotationally symmetric rf multipole traps is taken at the point, where the symmetry axis crosses this pseudopotential surface. In the case of the rf octupole trap, the dynamics even in the pseudopotential approximation exhibits a mainly chaotic behavior, showing ergodicity and mixing. Therefore, in the course of time each particle will nearly reach this maximum value of $\eta(\vec{r})$. Thus a maximum value of $\eta(\vec{r})$ can be assigned to the trap, considering the surface of $\eta(\vec{r})$ that touches the electrode structure of the trap. For stable trapping conditions, first the pseudopotential well depth should be high compared to the energy of the ions. Second, it is found empirically that the stability function $\eta(\vec{r})$ should not exceed $\eta_{\max} \leq 0.3$.

We may consider the trapped particle in an rf multipole trap undergoing sequences of uncorrelated collisions with the strong rf field in the outer regions of the trap, with all collisions changing the energy of the particle.

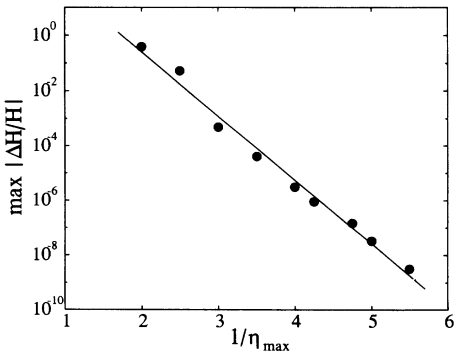

FIG. 4. Change of the kinetic energy of particles returning after a reflection in the outer region of an rf octupole trap back to the trap's center, plotted as a function of the inverse maximum value of the stability function along the particles trajectories.

The trajectory of a particle is then governed by a random walk which results in an effective diffusion of the initial energy [21]. Therefore even particles with low initial energies and corresponding low initial maximum values of $\eta_{\max}$ can leave the trap after a sufficient long time. This energy diffusion is the basic mechanism of rf heating which appears also as a consequence of space charge of ion clouds in Paul traps [9,8,26]. As can be inferred from Fig. 4, the rate at which rf heating occurs can be lowered by slightly increasing both the rf frequency and the rf voltage, thus lowering the maximum value of $\eta(\vec{r})$.

For the rf octupole potential (7), the pseudopotential (15) takes the following form in cylindrical coordinates:

$$\Psi(\rho,z,\varphi)=\frac{qV_0^2}{16m\Omega^2 s^8}(9\rho^6+78\rho^4z^2-48\rho^2z^4+64z^6), \tag{18}$$

and for the stability function $\eta(\vec{r})$ we obtain from Eq. (11)

$$\eta(\rho,z,\varphi)=\frac{3qV_0}{m\Omega^2 s^4}\left[\frac{81\rho^{10}+1440\rho^8z^2+480\rho^6z^4+2560\rho^4z^6-3840\rho^2z^8+4096z^{10}}{9\rho^6+76\rho^4z^2-48\rho^2+64z^6}\right]^{\frac{1}{2}}. \tag{19}$$

Contours of the pseudopotential Ψ and the stability function $\eta(\vec{r})$ are shown for Ba^+ ions in Figs. 5(a)–5(c). In each figure one quadrant of a ρ-z section through the rf octupole trap is shown with the shape of electrodes indicated by hatches. Dashed-dotted curves indicate equipotential lines and the solid lines indicate values of the stability parameter η.

A close inspection of the figures as presented in Figs. 5(a)–5(c) yields the following: optimum storage conditions are achieved for the rf octupole trap if the region with sufficient depth of the pseudopotential overlaps well with that allowing for motional stability. Figure 5(b) represents this situation. For rf voltages too small, the ion motion is stable over most of the trap's volume but ions can reach the trap electrodes since the pseudopotential well depth may be too small. This situation is shown in Fig. 5(a) and corresponds to the region of small scaled voltages, i.e., $q_4 < 0.1$ in Fig. 3 with its decreasing acceptance. By contrast, for rf voltages too high, the effective trapping volume becomes small since the motional stability of ions far from the trap center is limiting the storage capacity of the trap. This is shown in Fig. 5(c), corresponding to the region of high scaled voltages $q_4 > 0.1$ in Fig. 3.

V. SPACE CHARGE DISTRIBUTION IN AN ANHARMONIC PSEUDOPOTENTIAL

Before investigating the spatial distribution of ion clouds in rf multipole traps, subsequently modeled by the pseudopotential (15), we shall first give a heuristic argument how the density distribution is expected to be. The space charge potential $\Phi_{SC}(\vec{r})$ of an ion cloud and the distribution $n(\vec{r})$ of ions in the trap are related to each other by Poisson's equation, i.e.,

$$\Delta\Phi_{SC}(\vec{r})=-\frac{q}{\varepsilon_0}n(\vec{r}). \tag{20}$$

Since the Laplacian basically denotes the second derivative with respect to position, it follows from Eq. (20) that inside a constant-density distribution of charged particles

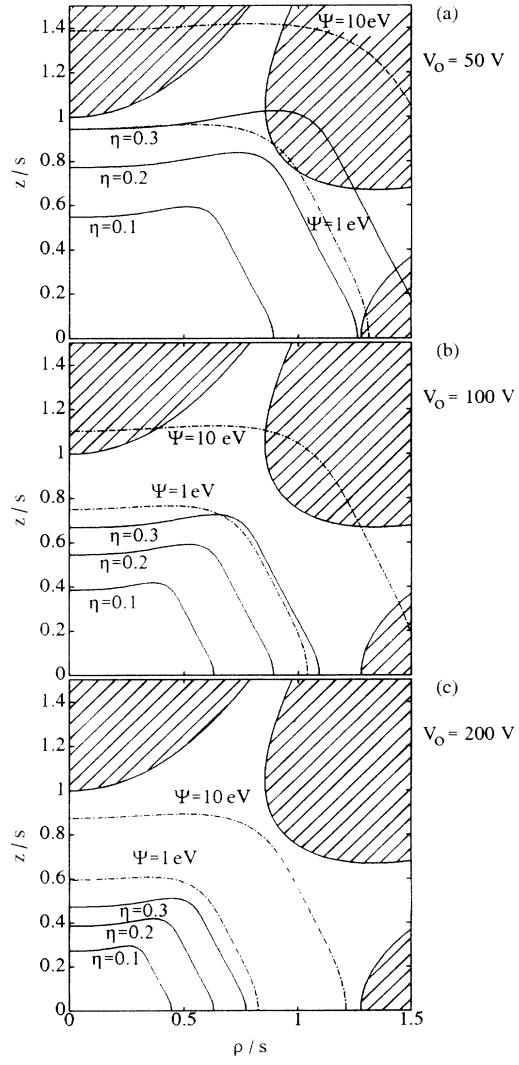

FIG. 5. Contours of the pseudopotential Ψ and stability function η for Ba^+ ions for one quadrant of the octupole potential, the electrodes are indicated by the hatches. (a) $V_0 = 50$ V, (b) $V_0 = 100$ V, (c) $V_0 = 200$ V.

a defocusing harmonic space charge potential is generated. Hence, in order to confine a constant-density ion distribution, a harmonic (effective) trapping potential is required which is generated by a Paul trap [18,19]. Considering an initially constant density-distribution of an ion cloud in a rf octupole trap, described by an anharmonic pseudopotential, the harmonic defocusing space charge potential dominates near the trap center over the trapping potential. This results in an equilibrium density distribution which is small near the center of the trap and increases to a maximum at some distance, where the extension of the ion cloud is limited, e.g., by beginning motional instability [10].

In order to include effects due to the temperature of the ion cloud, we now consider an equilibrium distribution of the ion density given by

$$n(\vec{r}) = n_0 \exp\left[-\frac{q}{kT}(\Psi(\vec{r}) + \Phi_{SC}(\vec{r}))\right]. \tag{21}$$

Here n_0 denotes the ion density at the center of the trap. By removing the space charge potential $\Phi_{SC}(\vec{r})$ from the system of Eqs. (20) and (21), we obtain a nonlinear partial differential equation

$$\Delta\left[\frac{kT}{q}\ln\frac{n(\vec{r})}{n_0} + \Psi(\vec{r})\right] = \frac{q}{\varepsilon_0}n(\vec{r}), \tag{22}$$

which can be used to obtain the density distribution of the ion cloud, provided the pseudopotential $\Psi(\vec{r})$ of the ion trap, the temperature T, and the total number of stored particles n_0 are given [22–24]. Considering the limiting case of vanishing temperature, $T \to 0$, the density distribution is readily obtained to be [22,23]

$$n(\vec{r}) = \frac{q}{\varepsilon_0}\Delta\Psi(\vec{r}). \tag{23}$$

In contrast, for the limiting case of high ion temperatures, the density distribution of the ion cloud is given by [22,23]

$$n(\vec{r}) = n_0 \exp\left[-\frac{q\Psi(\vec{r})}{kT}\right]. \tag{24}$$

For temperatures in between these two limiting cases, the density distribution of ion clouds has to be determined numerically. We investigated the ion-density distribution given by Eq. (22) numerically for two simple pseudopotentials, i.e., for

$$\Psi(\vec{r}) = \Psi(R_0)\left(\frac{r}{R_0}\right)^{2k}, \tag{25}$$

with $k = 1$ and $k = 3$. The first case is related to the spherical pseudopotential which can be generated using an rf quadrupole trap with appropriate dc voltage [18], while the second case gives a spherical pseudopotential of the same power as the pseudopotential of the rf octupole trap, given by Eq. (18). That is, for simplicity we neglect that the pseudopotential, as given by Eq. (18), depends on the polar angle. For a comparison with previous results for rf quadrupole traps, parameters were chosen in a way to reproduce the situation of Fig. 1 in Ref. [23], i.e., $\Psi(R_0 = 10\text{ mm}) = 10.18$ V and the total number of ions $N = 10^6$. Figure 6(a) shows the ion-density distribution for the spherical pseudopotential of an rf quadrupole trap, essentially reproducing Fig. 1 of Ref. [23], and Fig. 6(b) for the spherical pseudopotential, proportional to r^6 as an approximation of an rf octupole trap. For the harmonic pseudopotential, with increasing temperature the ion density evolves from a constant-density distribution, as suggested by Eq. (23), to a Gaussian density distribution, as suggested by Eq. (24) [23,25]. By contrast, in an anharmonic pseudopotential, for high temperatures a flattened distribution of ions is obtained, while for intermediate and low temperatures, the ion density becomes low near the trap center and has a maximum at some distance to the trap's center.

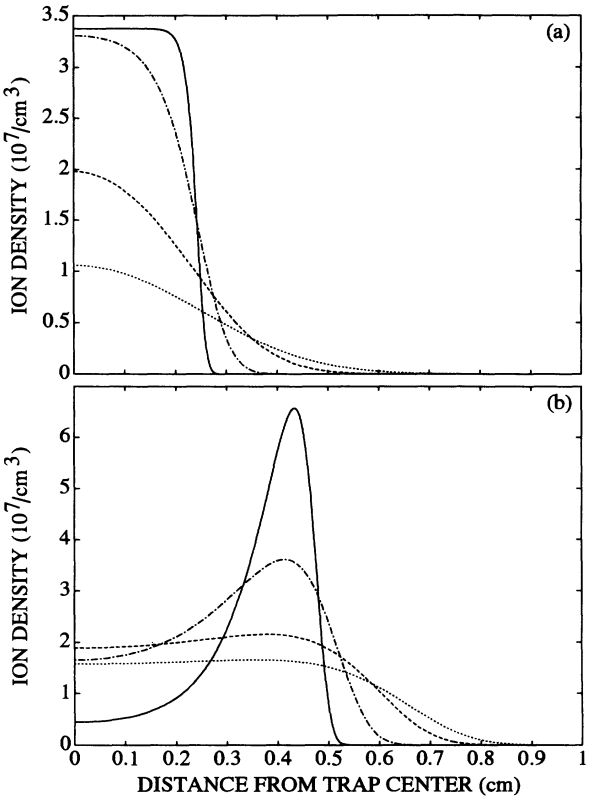

FIG. 6. Ion density distribution for a spherical pseudopotential of an rf quadrupole trap (a) and pseudopotential proportional to r^6 as an approximation of the rf octupole trap. Parameters: T = 100 K (solid line), T = 1000 K (dashed-dotted line), T = 5000 K (long dashes), and T = 10000 K (short dashes).

VI. EXPERIMENTAL SETUP

In our experiments, clouds of Ba^+ ions were stored in an rf octupole trap with a characteristic dimension s = 17.6 mm. The trapping rf voltage at frequencies between 300 kHz and 600 kHz was varied up to 2 kV_{pp}. Since the experimental setup otherwise is the same as used for investigations of the dynamics of ion clouds in rf quadrupole traps (Paul traps) [26–29], it will be described

here only briefly.

Relevant to our experiment are the $6\,^2S_{1/2}$, $6\,^2P_{1/2}$, and the $5\,^2D_{3/2}$ states of the Ba^+ ion, forming a Λ-type three-level scheme. Light from a dye laser at 493 nm excites the Ba^+ ion from the $6\,^2S_{1/2}$ ground state to the $6\,^2P_{1/2}$ state. The P state decays with a branching ratio of about 2.85:1 either back to the ground state or to the metastable $5\,^2D_{3/2}$ state. Light from a second dye laser at 650 nm excites ions from the D states, thus avoiding optical pumping.

The laser beams collinearly cross the ion cloud via holes drilled in the central ring and the resulting resonance fluorescence on the S-P transition is observed through the upper endcap, which is formed from a mesh. A photomultiplier detects light at 493 nm, stray light as well as resonance fluorescence at 650 nm is suppressed by means of a colored glass filter. Stray light at 493 nm is suppressed by lock-in detection. For that, the laser beam at 650 nm is periodically chopped, which causes immediate optical pumping to the D state. Thus resonance fluorescence at 493 nm vanishes and lock-in detection separates the periodically varying resonance fluorescence from the continous stray-light background at 493 nm.

The rf octupole trap, an electron gun, and an atomic beam source are placed in a vacuum chamber with background pressures smaller than 10^{-5} Pa. Inside the trap, ions are created from the atomic beam by electron impact ionization. A loading time of 20 s is sufficient to completely fill the ion trap. In our experiment, mechanically blocking the atomic beam from entering the trapping volume after loading the trap proved to be essential to obtain proper steady-state conditions for an ion cloud.

VII. LINE SHAPE OF OBSERVED EXCITATION SPECTRA

Figure 7 shows an observed excitation spectrum of an ion cloud in the rf octupole trap; the trapping voltage was 500 V_{pp} at $\Omega/2\pi = 400$ kHz. The red light field at 650 nm was tuned to the center frequency of the D-P transition, while the green light field was tuned across the S-P resonance. In the center of the spectrum, the frequency difference of the two laser light fields is resonant with the energy spacing between the S and the D levels. Thus two-photon transitions can form a coherent superposition of the S and the D states, leaving the P state without occupation and hence the resonance fluorescence at 493 nm decreases. This is the well known "dark resonance" in Λ-type three-level systems due to coherent population trapping [4]. Due to the motion of Ba^+ ions in the rf octupole trap the excitation spectrum is strongly broadened compared with the natural linewidth of the P state, which is $\Gamma_P/2\pi = 20.4$ MHz. Aside from the dark resonance, excitation spectra observed on ion clouds in rf quadrupole traps are known to have a Gaussian shape [26,27]. The line shapes observed from ion clouds in the rf octupole trap exhibit as a characteristic feature — especially for low rf voltages — a narrow peak on a broader pedestal. This can be explained as follows: since motional frequencies of ions confined in the rf octupole trap are always less or equal to the trap's driving frequency (i.e., 300–650 kHz), emission and absorption of photons (with time scales of several ns) are very fast processes on the time scale of the ion motion. Hence characteristic features of observed excitation spectra mirror simply the ion motion in the trap. Since the pseudopotential of the rf octupole trap corresponds to that of a hardening spring, ion trajectories between reversions show extended straight sections (cf. also Fig. 2). The trapping field then has little influence on the ion motion, and both laser frequencies have to coincide with the ionic transition frequencies within a width given by the natural linewidth and saturation broadening to provide sufficient occupation in the P state. For free particles this is achieved only for a few velocity classes, resulting in excitation spectra with linewidths much smaller than the Doppler width (cross saturation) [27]. Consequently we refer to particles near the trap center as quasifree particles. On the other hand, while the ion motion reverses, the micromotion amplitude is large since the ion is maximally elongated with respect to the trap center (cf. Fig. 2), resulting in a broad Gaussian pedestal of the line shape, as is observed in the case of an rf quadrupole trap [27]. Therefore the observed spectra, as e.g., shown in Fig. 7, result from an ion ensemble which shows in parts a free-particle behavior and also shows the trapped-particle behavior indicated by the broad background.

Figure 8 shows observed excitation spectra of ion clouds in the rf octupole trap as a function of the trapping voltage, the dark resonances being not resolved. It can be seen from Fig. 8 that the narrow central peak disappears for high trapping voltages. Increasing the rf voltage causes an overall increase of the micromotion thus reducing the quasifree sections of the ion motion. According to the discussion above, for high rf voltages the narrow central peak is dominated by the Gaussian pedestal, with a linewidth corresponding to the full Doppler width of the ion motion [27].

The following investigation of the dynamics of ion clouds in the rf octupole trap in Sec. VIII below relies on information obtained from observed excitation spectra as follows: the mean kinetic energy of an ion cloud is determined from the Doppler width of the Gaussian pedestal,

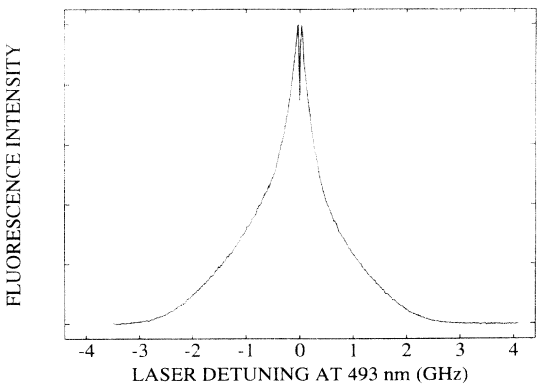

FIG. 7. Excitation spectrum of a trapped cloud of Ba^+ ions.

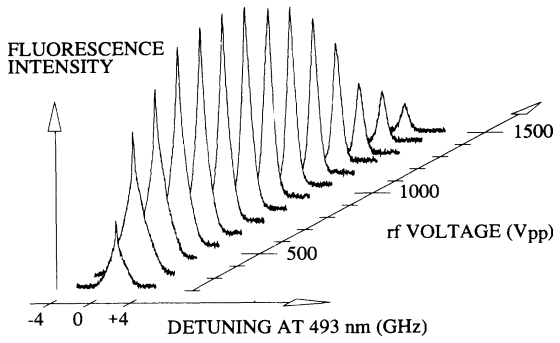

FIG. 8. Excitation spectra as a function of the trapping rf voltage at a driving frequency $\Omega/2\pi = 400$ kHz. The spectra were taken about 3 min after filling the trap.

since the linewidth of the central peak is narrowed by cross-saturation effects [27]. Further, as a measure for the mean total number of ions in the rf octupole trap, we determined the area covered by the observed excitation spectra. This procedure neglects that optical pumping to the D level and coherence effects, as e.g., dark resonances, may reduce the resonance fluorescence during the straight sections of the ion motion (quasifree motion), which occurs predominantly for low rf voltages. To correct this systematic error, however, one would have to know the occupation probability of the D state as a function of the ion motion, which is not easily accessible for the case of an ion cloud. Thus the height of the central narrow peak is at worst underestimated and hence the derived features, as e.g., the (quasifree) ion number, are conservatively determined and present at worst a lower limit.

VIII. MEAN KINETIC ENERGY AND RELATIVE PARTICLE NUMBER AS A FUNCTION OF THE TRAPPING PARAMETERS

Figures 9(a) and 9(b) display the relative number and the mean kinetic energy of trapped ion clouds as a function of the trapping rf voltage at $\Omega/2\pi = 400$ kHz. As can be seen from Fig. 9(a), the relative number of trapped particles is nearly constant in time for low rf voltages. This corresponds to motional stability over most of the trap's volume according to Fig. 5(a). However, since the pseudopotential is fairly low, maximum particle numbers are not stored for these (low) rf voltages but for voltages in the range of 400 to 600 V_{pp} at $\Omega/2\pi$ =400 kHz. For rf voltages higher than 600 V_{pp}, more than 10% of the ions are lost within 2 min. This instability of ion confinement in time corresponds to the small spatial region of motional stability in Fig. 5(c). The overall shape of Fig. 9(a) agrees well with transmission curves obtained experimentally from a linear rf octupole beam guide [15].

Figure 9(b) shows the mean kinetic energy of an ion cloud 2.5 min after the ions were loaded to the trap as a function of the rf voltage at 400 kHz. Again, important features of the curve can be explained qualitatively by following the analysis of Sec. IV. When the rf voltages increase primarily the pseudopotential well depth increases while motional stability is still preserved for most of the trap's volume. The total number of trapped particles hence increases [cf. Fig. 9(a)] and so does the mean kinetic energy. With rf voltages increasing further, the spatial region allowing for motional stability diminishes. Accordingly, the height of the pseudopotential useful for confinement of ions decreases [cf. Fig. 5(c)], and so does the mean kinetic energy, since the most energetic ions evaporate from the ion cloud first.

At this point, it might be interesting to compare rf and dc voltages and search for optimum parameters as is done in the case of the rf quadrupole trap [30]. The stability diagram for the rf quadrupole trap (Paul trap) does not contain the point of zero rf trapping voltage due to space charge effects [31]. To our opinion, a similar space charge shift prevents that we obtain quantitative agreement between the theoretical analysis of Sec. IV (where single ion trajectories were calculated) and the observed experimental results.

By comparing the storage properties of the rf octupole trap with that of an rf quadrupole trap [26] of the same size (i.e., the same ring diameter) and similar volume, we are led to the following conclusion: optimum storage conditions for ion clouds in the rf quadrupole trap (i.e., maximum total number of ions) are achieved at scaled voltages of about $a_z = -0.03$ and $q_z = 0.55$ [30]. The

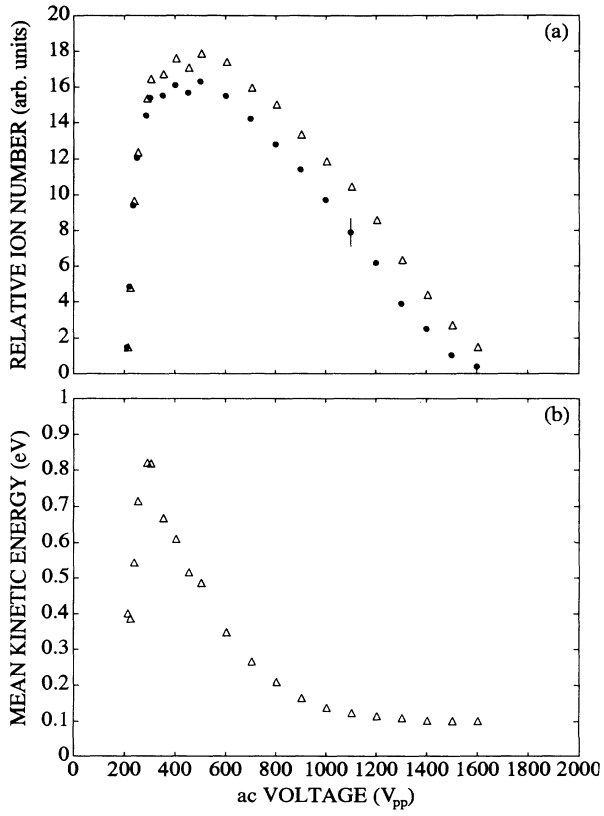

FIG. 9. Relative ion number (a) and mean kinetic energy (b) as a function of the ac trapping voltage V_0. The relative number in (a) is shown for times of two minutes (filled circles) and four minutes (triangles) after loading a new ion cloud to the trap.

range of scaled rf voltages q_z, where clouds of Ba^+ ions have been detected with rf quadrupole traps used in [26] extends from $q_z \simeq 0.37 - 0.98$ at zero dc voltage [32]. For our rf octupole trap, the range of scaled rf voltages q_4 extends from $q_4 \simeq 0.1 - 0.81$, with significant losses of ions beginning at $q_4 \simeq 0.3$. Compared to the rf quadrupole trap, the total range of rf voltages, allowing for confinement of ions in the rf octupole trap, is larger and centered at lower rf voltages.

Note that the pseudopotential of an rf octupole trap is proportional to r^6, while a dc octupole potential is proportional to r^4. A dc octupole potential, if added to the rf octupole potential deforms the trap's pseudopotential in a complicated manner of no evident advantage. Experimentally, nonzero dc octupole potentials were observed not to improve the trapping stability, but to reduce the number of stored ions. By contrast, for the rf quadrupole trap, both the pseudopotential and the dc potential are proportional to r^2, but have different dependencies on the polar angle. Therefore, the dc voltage can be adjusted to form a total pseudopotential of spherical symmetry [18] which may be of advantage for ion confinement. This is not possible in the rf octupole trap and all subsequent measurements were taken for zero dc potentials.

Figures 10(a) and 10(b) show the relative number of trapped ions and the mean kinetic energy of ion clouds in the rf octupole trap as a function of the squared frequency $\Omega/2\pi$. For these curves, both the trap's driving frequency and the trapping rf voltage were varied such that the ratio V_0/Ω^2 remained constant. Hence the stability function η is kept at a fixed value, while the depth of the pseudopotential increases with increasing Ω [26]. All measurements indicated in Figs. 10(a) and 10(b) were taken 2.5 min after loading the trap, which ensured that quasistationary conditions are reached. As is seen from Figs. 10(a) and 10(b), both the total number of ions and the mean kinetic energy of ion clouds increase linearly with the square of the trapping frequency $\Omega/2\pi$. Such a behavior has been similiarly observed for rf quadrupole traps, provided the stability function (in this case q_r, q_z) is kept constant [26].

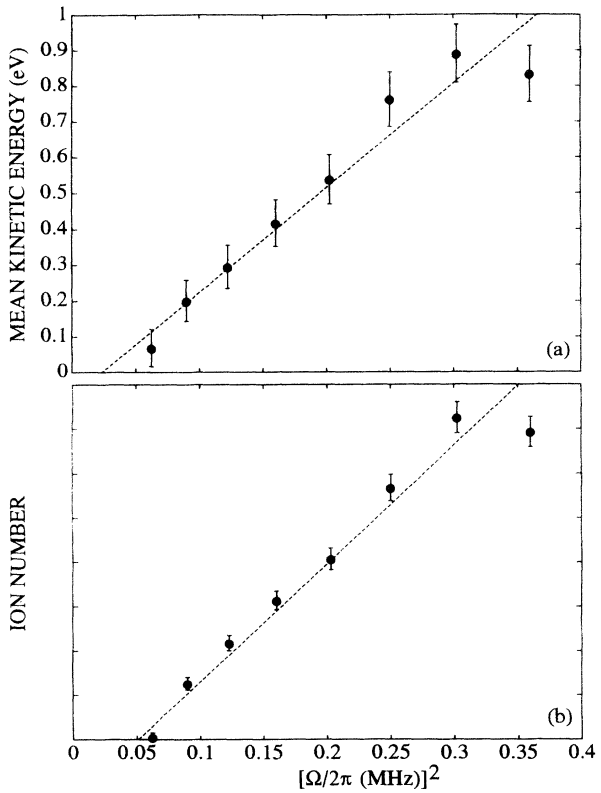

FIG. 10. Mean kinetic energy and relative ion number as a function of the square of the driving frequency $\Omega/2\pi$.

IX. OBSERVED SPATIAL DISTRIBUTION OF TRAPPED ION CLOUDS

For a measurement of the spatial distribution of the fluorescence intensity of stored ion clouds in the rf octupole trap, we took photographs of the fluorescing ion cloud [28]. The photographs have been evaluated using a microdensitometer and by employing a calibration curve which allowed us to obtain the fluorescence intensity from the optical density of the film. Figure 11 shows a measurement of the spatially resolved fluorescence intensity of a stored ion cloud at an rf voltage of 1125 kV_{pp} at $\Omega/2\pi = 600$ kHz. Both lasers were tuned to resonance. The two distinct maxima correspond to maxima of the ion density caused by Coulomb repulsion in the anharmonic pseudopotential of the octupole trap, as discussed in Sec. V. The asymmetry of Fig. 11 with respect to the trap center is due to unintentionally focusing the laser beams to the right hand side of the trap. This produces a spatially varying light intensity of the laser beam and causes the higher peak on the right. At the trap center, the fluorescence intensity shows a minimum corresponding to a dark zone orthogonal to the direction of propagation of the light fields [26] due to spatially localized optical pumping [28]. All the spatially resolved measurements show a similar shape as shown in Fig. 11. Hence, as a measure for the spatial extension of the ion clouds, the separation of the two distinct maxima was evaluated from the observed fluorescence distribution. Note that

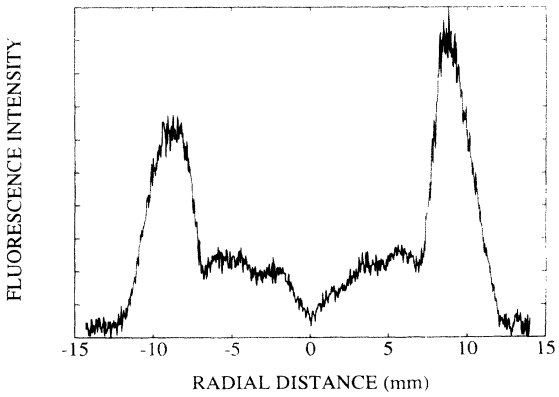

FIG. 11. Spatially resolved fluorescence of an ion cloud in the rf octupole trap. Parameters: trapping voltage $V_0 = 1125$ V_{pp}, $\Omega/2\pi = 600$ kHz.

an ion cloud in a Paul trap has a Gaussian spatial distribution with an extension which is much smaller than the distance between the two distinct maxima observed in the octupole trap [26].

X. POSITION DEPENDENCE OF THE TRAPPING STABILITY

Figure 12 shows the spatial extension of ion clouds in the rf octupole trap as a function of the rf voltage at $\Omega/2\pi = 400$ kHz with both lasers tuned to resonance. The observed spatial extension may be compared to twice the maximum extension from the center of the trap allowing for stable ion motion. This is shown in Fig. 12 by dashed curves for different values of the stability function η in radial direction, as given by Eq. (19). As discussed in Sec. IV, the value of η should not exceed 0.3 [12]. From Fig. 12 it can be seen that the observed spatial diameter of the fluorescing part of the ion cloud—as obtained from measurements with both lasers tuned to resonance—is lower than the limit posed by the condition $\eta \leq 0.3$ for stable ion motion. This behavior is especially pronounced for the lower rf voltages in Fig. 12 where the flatness of the trap's pseudopotential but not the motional instability is limiting the storage capacity of the rf octupole trap [cf. Figs. 5(a)–5(c)]. For higher rf voltages, the observed maximum extension of the fluorescing part of the ion cloud agrees better with the limit posed by $\eta \leq 0.3$, indicating that for higher rf voltages motional instability is limiting the storage capacity of the trap, as discussed in Sec. IV. However, all the observed spatial extensions in Fig. 12 are systematically lower than the limit set by $\eta \leq 0.3$ due to the following effect: with both lasers tuned to resonance, only ions with velocities around zero may be effectively excited by the laser-light fields and contribute to the observed fluorescence. Due to the large distance from the trap center, ions at the outer side of the ion cloud have high velocities (due to their strong micromotion). For the lasers tuned to resonance, those ions contribute very little to the observed fluorescence. Consequently, the spatial extension of the ion clouds are systematically underestimated in a measurement with both lasers tuned to resonance.

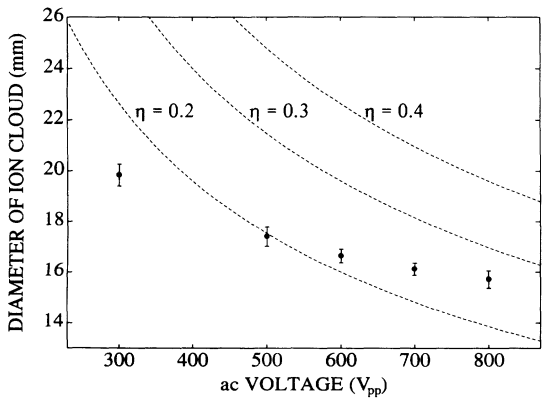

FIG. 12. Diameter of the ion cloud as a function of the ac trapping voltage. The dashed lines indicate values of constant η values.

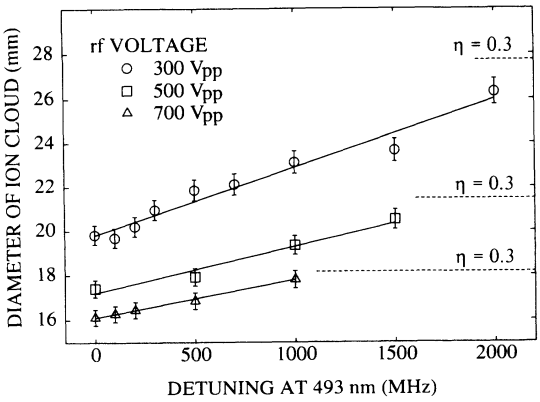

FIG. 13. Diameter of the fluorescing part of an ion cloud as a function of the laser detuning at 493 nm. Three curves are shown for different rf voltages at $\Omega/2\pi = 400$ kHz. Solid lines, resulting from linear regression, are drawn to guide the eye. Dashed lines indicate the limit for motional stability.

Figure 13 shows the spatial extension of ion clouds in the rf octupole trap as a function of the detuning of the laser at 493 nm. With increasing detuning, those ions which have higher velocity amplitudes and correspondingly have the highest distance from the trap center now can contribute to the observed fluorescence intensity [28]. Hence the spatial extension of the fluorescing part of the ion cloud increases with the detuning of the light field. With increasing rf voltage, the pseudopotential becomes steeper and the spatial extension of an ion cloud decreases, as shown in Fig. 13 by the three different curves. Also indicated in Fig. 13 is twice the distance from the trap center, for which the stability function η, as given by Eq. (19), equals 0.3 in the radial direction. The observed maximum extension of the ion cloud is in reasonable agreement with the limit posed by the requirement for motional stability. This agreement is especially good for the higher trapping rf voltages (i.e., the lower curve in Fig. 13), where motional instability is limiting

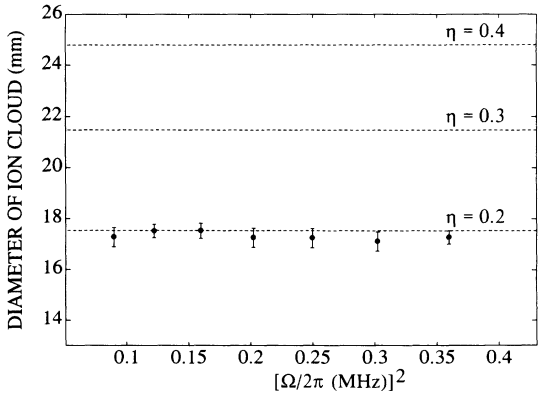

FIG. 14. Diameter of the ion cloud as a function of the squared driving frequency $\Omega/2\pi$. The dashed lines indicate values of the stability parameter η.

the storage capacity of the trap.

Figure 14 shows the observed spatial extension of ion clouds in the rf octupole trap as a function of the square of the frequency $\Omega/2\pi$. Both light fields were tuned to resonance. Again, both the trap's driving frequency and the trapping voltage were varied such that the ratio V_0/Ω^2 remained constant. As discussed in Sec. VIII, this procedure keeps the stability function η fixed and varies the depth of the pseudopotential. As expected, Fig. 14 shows that the observed spatial extension of ion clouds in the rf octupole trap does not depend on the depth of the pseudopotential, similar to the quadrupole case [29]. Also shown in Fig. 14 is twice the maximum extension from the trap center for three different limiting values of η (cf. dashed lines in Fig. 14). As discussed above, for both light fields tuned to resonance the observed spatial extension of the fluorescing part of the clouds is lower than the limit posed by the condition $\eta \leq 0.3$ for motional stability.

XI. CONCLUSION

Confinement and dynamics of ion clouds in an rf octupole trap have been investigated. The stability of a nonlinear parametric oscillator was investigated both theoretically by numerical integration of the equations of motion together with analytical arguments and experimentally by spatially resolved measurements of the fluorescence intensity. It was found that ions in an rf octupole trap should move near the center of the trap essentially as an ion gas unperturbed by the trapping field. Thus it should be possible to apply cooling techniques as they are known for atoms. We perceive the possibility to cool at least parts of such an ion cloud (near the center of the trap) using *optical molasses* techniques. This would give access to both a confined, laser-cooled, and weakly interacting ensemble as it is desirable for many spectroscopic experiments in the optical as well as in the microwave domain.

ACKNOWLEDGMENTS

We acknowledge continuous support by Professor P. E. Toschek. M.S. and I.S. acknowledge financial support from the Claussen-Stiftung. This work was supported by the Deutsche Forschungsgemeinschaft.

[1] See, e.g., J. Mod. Opt. **39**, 192 (1992), special issue on *The Physics of Trapped Ions*, edited by R. Blatt, P. Gill, and R. C. Thompson.
[2] J. C. Bergquist, W. M. Itano, and D. J. Wineland, Phys. Rev. A **36**, 428 (1987).
[3] F. Diedrich and H. Walther, Phys. Rev. Lett. **58**, 203 (1987).
[4] I. Siemers, M. Schubert, R. Blatt, W. Neuhauser, and P. E. Toschek, Europhys. Lett. **18**, 129 (1992).
[5] M. Schubert, I. Siemers, R. Blatt, W. Neuhauser, and P. E. Toschek, Phys. Rev. Lett. **68**, 3016 (1992).
[6] J. C. Bergquist, F. Diedrich, W. M. Itano, and D. J. Wineland, in *Laser Spectroscopy IX*, edited by M. S. Feld, J. E. Thomas, and A. Mooradian (Academic, San Diego, 1989), p. 274.
[7] W. Neuhauser, M. Hohenstatt, P. E. Toschek, and H. Dehmelt, Phys. Rev. A **22**, 1137 (1980).
[8] H. G. Dehmelt, in *Advances in Laser Spectroscopy*, edited by F. T. Arecchi, F. Strumia, and H. Walther (Plenum, New York, 1983).
[9] R. Blümel, C. Kappler, W. Quint, and H. Walther, Phys. Rev. A **40**, 808 (1989); **46**, 8034(E) (1992).
[10] D. J. Wineland, in *Proceedings of the Cooling, Condensation, and Storage of Hydrogen Cluster Ion Workshop, Menlo Park, CA*, edited by J. T. Bahns (SRI Stanford, CA, 1987); reprinted in *Trapped Ions and Laser Cooling II*, edited by D. J. Wineland, W. M. Itano, J. C Bergquist, and J. J. Bollinger, NIST Technical Note **1324**, TN-168 (U.S. GPO, Washington, D.C., 1988).
[11] J. Walz, I. Siemers, M. Schubert, W. Neuhauser, and R. Blatt, Europhys. Lett. **21**, 183 (1993).
[12] E. Teloy and G. Gerlich, Chem. Phys. **4**, 417 (1974).
[13] M. Okumura, L. I. Yeh, D. Normand, and Y. T. Lee, J. Chem. Phys. **85**, 1971 (1986).
[14] S. W. Bustamente, M. Okumura, D. Gerlich, H. S. Kwok, L. R. Carlson, and Y. T. Lee, J. Chem. Phys. **86**, 508 (1987).
[15] P. Tosi, G. Fontana, S. Longano, and D. Bassi, Int. J. Mass Spectrom. Ion Proc. **93**, 95 (1989).
[16] I. Szabo, Int. J. Mass Spectrom. Ion Proc. **73**, 197 (1986); C. Hägg and I. Szabo, *ibid.* **73**, 237 (1986); **73**, 277 (1986); *ibid.* **73**, 295 (1986).
[17] R. D. Knight, Int. J. Mass Spectrom. Ion Phys. **51**, 127 (1983); D. J. Wineland and H. G. Dehmelt, J. Appl. Phys. **46**, 919 (1975).
[18] D. J. Wineland, W. M. Itano, and R. S. VanDyck, Jr., Adv. At. Mol. Phys. **22**, 135 (1983); P. E. Toschek, in *New Trends in Atomic Physics*, Les Houches Session XXXVIII, edited by G. Grynberg and R. Stora (Elsevier Science Publishers B.V., Amsterdam, 1984), p. 381.
[19] H. G. Dehmelt, Adv. At. Mol. Phys. **3**, 53 (1967); **5**, 109 (1969).
[20] L. D. Landau, and E. M. Lifshitz, *Mechanics* (Pergamon Press, Oxford, 1960).
[21] E. Teloy (unpublished).
[22] E. S. Weibel and G. L. Clark, J. Nucl. Energy Part C **2**, 112 (1961).
[23] L. S. Cutler, C. A. Flory, R. P. Giffard, and M. D. McGuire, Appl. Phys. B **39**, 251 (1986).
[24] E. Teloy (unpublished).
[25] C. Meis, M. Desaintfuscien, and M. Jardino, Appl. Phys. B **45**, 59 (1988).
[26] I. Siemers, R. Blatt, Th. Sauter, and W. Neuhauser, Phys. Rev. A **38**, 5121 (1988).
[27] M. Schubert, I. Siemers, and R. Blatt, Phys. Rev A **39**, 5098 (1989).
[28] M. Schubert, I. Siemers, and R. Blatt, J. Opt. Soc. Am. B **6**, 2154 (1989).
[29] M. Schubert, I. Siemers, and R. Blatt, Appl. Phys. B **51**, 414 (1990).
[30] R. Iffländer and G. Werth, Metrologia **13**, 167 (1977).
[31] E. Fischer, Z. Phys. **156**, 1 (1959).
[32] I. Siemers, R. Blatt, Th. Sauter, and W. Neuhauser (unpublished).